Multidecadal Variations in the Relationship between the NAO and Winter Precipitation in the Hindu Kush–Karakoram

LUCA FILIPPI

Institute of the Atmospheric Sciences and Climate ISAC-CNR, and Dipartimento di Ingegneria Meccanica e Aerospaziale, Politecnico di Torino, Torino, Italy

ELISA PALAZZI, JOST VON HARDENBERG, AND ANTONELLO PROVENZALE

Institute of the Atmospheric Sciences and Climate, ISAC-CNR, Torino, Italy

(Manuscript received 18 April 2014, in final form 21 July 2014)

ABSTRACT

Winter precipitation over the Hindu Kush–Karakoram (HKK) range in the western Himalayas is generated by westerly perturbations whose dynamics is affected by the North Atlantic Oscillation (NAO). Larger precipitation is typically recorded during the positive NAO phase. In this work, the relationship between the NAO and winter precipitation in the HKK is explored further, using an ensemble of precipitation datasets and the 40-yr ECMWF Re-Analysis (ERA-40) and Twentieth Century Reanalysis (20CR) data. The mechanisms underlying this relationship are discussed, with a focus on the secular variations that occurred in the last century. The NAO exerts its control on HKK precipitation by altering the intensity of westerly winds in the region of the Middle East jet stream (MEJS). Results indicate that evaporation from the Persian Gulf, the northern Arabian Sea, and the Red Sea plays an important role. During positive NAO phases, westerlies are strengthened and enhanced evaporation occurs from these basins owing to higher surface wind speed. The extra moisture combines with stronger westerlies and results in enhanced moisture transport toward the HKK. Precipitation datasets covering the twentieth century show an alternation of periods of strong and weaker influence of the NAO on precipitation in the HKK. It is found that these variations are associated with changes in the spatial pattern of the NAO: the relative position of the two centers of action of the NAO determines to what extent it can modulate the MEJS, affecting precipitation in the HKK.

1. Introduction

The Hindu Kush–Karakoram (HKK) range, encompassing parts of Afghanistan, Pakistan, India, and China, is at the western edge of the Himalayan range, the largest mountain region in the world.

The whole Himalayan region is exposed to three main circulation patterns—the Indian summer monsoon, the East Asian monsoon, and westerly perturbations, also called western weather patterns (WWPs) (Archer and Fowler 2004; Syed et al. 2006; Yadav et al. 2012; Pal et al. 2014)—leading to different precipitation climatologies in the western, central, and eastern portions of the mountain chain (Bookhagen and Burbank 2010). The HKK in the west is strongly impacted by westerly perturbations originating from the Mediterranean/Atlantic regions during winter and it is affected, at least in part, by the monsoon during summer. As a result, precipitation in the HKK is characterized by a bimodal annual cycle (Palazzi et al. 2013). In the western Himalaya and in the Karakoram, WWPs are primarily responsible for the build-up of seasonal snow cover, which represents a crucial water reservoir and a significant source for some of the major river basins in the region, such as the Indus River and its tributaries (Archer and Fowler 2004). Bookhagen and Burbank (2010) showed that snowmelt constitutes up to 50% of the total annual discharge in this area.

The North Atlantic Oscillation (NAO) is the dominant pattern of atmospheric variability in the North Atlantic sector and it refers to changes in the intensity and location of the Azores pressure high in the subtropical Atlantic and of the Icelandic low in the Arctic. It strongly affects climate across much of the Northern

Corresponding author address: Luca Filippi, ISAC-CNR, Corso Fiume, 4, 10133 Turin, Italy.
E-mail: l.filippi@isac.cnr.it

DOI: 10.1175/JCLI-D-14-00286.1

Hemisphere during winter (Hurrell et al. 2003). Some authors have regarded the NAO as the regional expression of a hemispheric, zonally symmetric mode of variability known as the Arctic Oscillation (AO) or northern annular mode (NAM) (see, e.g., Thompson and Wallace 2001). While there is an ongoing debate about the relationship between the NAO and AO (Wallace 2000; Ambaum et al. 2001), their time series show strong similarities, and Deser (2000) found a temporal correlation of 0.95 between the two for monthly data. For this reason, here we focus on the North Atlantic Oscillation but we would reasonably expect similar findings if an index measuring the AO were adopted instead.

Recently the NAO has been indicated as an important regulating factor also in the Karakoram region (Syed et al. 2006; Yadav et al. 2009b). Previous work has focused on the effects of the NAO on winter precipitation in the HKK based on the analysis of data from individual in situ stations (Archer and Fowler 2004), spatial averages of ground measurements (Yadav et al. 2009b), or gridded datasets (Syed et al. 2006). All studies agreed in showing that winter precipitation and the NAO are correlated with above (below) normal precipitation over the HKK area during the positive (negative) NAO phase.

Two mechanisms have been proposed to explain the link between the NAO and precipitation in the HKK. Syed et al. (2010) observed an increase in the number and intensity of eastern Mediterranean storms reaching northern Pakistan during the positive NAO phase, as the result of deeper surface and 500-hPa troughs over central-southwestern Asia in that phase. They also noticed that the transport of extra moisture during the positive NAO phase from the Mediterranean, the Caspian, and the Arabian Seas contributes to the NAO-related precipitation signal in northern Pakistan. Another mechanism was proposed by Yadav et al. (2009b) in which WWPs are intensified over northwestern India by the strengthening of the westerly jet stream over the Middle East during the positive NAO phase.

The relationship between the NAO and precipitation in the HKK underwent secular variations during the twentieth century. Yadav et al. (2009b) investigated the temporal evolution of this relationship, finding significant correlations between the NAO and precipitation in the period from 1940 to 1980 and nonsignificant ones in the first and last part of the century. The recent drop in the NAO control was accompanied by a simultaneous strengthening of the relationship between El Niño–Southern Oscillation (ENSO) and precipitation in this area, which was not significant in the period 1940–80. Yadav et al. (2010) showed that the intensification of the ENSO signal in recent decades was associated with a change in the strength of the tropical atmospheric response to ENSO. This result, at least in part, can also explain the recent weakening of the NAO–precipitation relationship. However, it is not clear if the secular variations in the NAO–precipitation relationship can be attributed entirely to changes in the intensity of the ENSO signal. Figure 2 in Yadav et al. (2009b) shows periods (before 1920 and between 1930 and 1940) when neither the NAO nor ENSO was statistically linked to precipitation in this area, suggesting that while ENSO could be a factor, there must also be other processes able to determine such variations.

The NAO underwent notable changes in the late 1970s. In particular, it shifted from a predominance of the negative phase in the 1960s to a predominance of the positive phase in the 1990s. Many studies showed that this trend is outside the range of internal atmospheric variability (Thompson et al. 2000; Feldstein 2002; Gillett et al. 2003). At the same time, Hilmer and Jung (2000) and Lu and Greatbatch (2002) documented an eastward displacement of the centers of action (COAs) of interannual variability of the NAO in the period 1978–97 compared to the previous decades. The extent to which these concurrent changes are linked to each other is still a matter of debate (see, e.g., Luo et al. 2010). In any case, a spatial shift in the NAO variability has strong implications for different climatic parameters (Jung et al. 2003; Pinto and Raible 2012). Wang et al. (2012) investigated the spatial displacements of the NAO COAs on decadal time scales from the end of the nineteenth century onward. They introduced a new climate index [the angle index (AI)] to quantify the relative position of the COAs in 20-yr running windows and showed that the AI provides additional information that cannot be represented by a standard, fixed-in-space NAO index. All of these changes, at least in principle, may have played a role also in the secular variations of the NAO–precipitation signal.

In this work, we investigate the relationship between the NAO and precipitation in the HKK region (shown in Fig. 1) using an ensemble of precipitation datasets, including three gridded archives based on the interpolation of in situ rain gauge measurements [the Global Precipitation Climatology Centre (GPCC), Climate Research Unit (CRU), and Asian Precipitation Highly-Resolved Observational Data Integration Toward Evaluation of Water Resources (APHRODITE) datasets] and the 40-yr European Center for Medium-Range Weather Forecasts (ECMWF) Re-Analysis (ERA-40). The complex orography of the region, the sparse coverage of ground stations, usually limited to lower altitudes, and issues in properly measuring solid precipitation are major constraints for precipitation estimates in this area

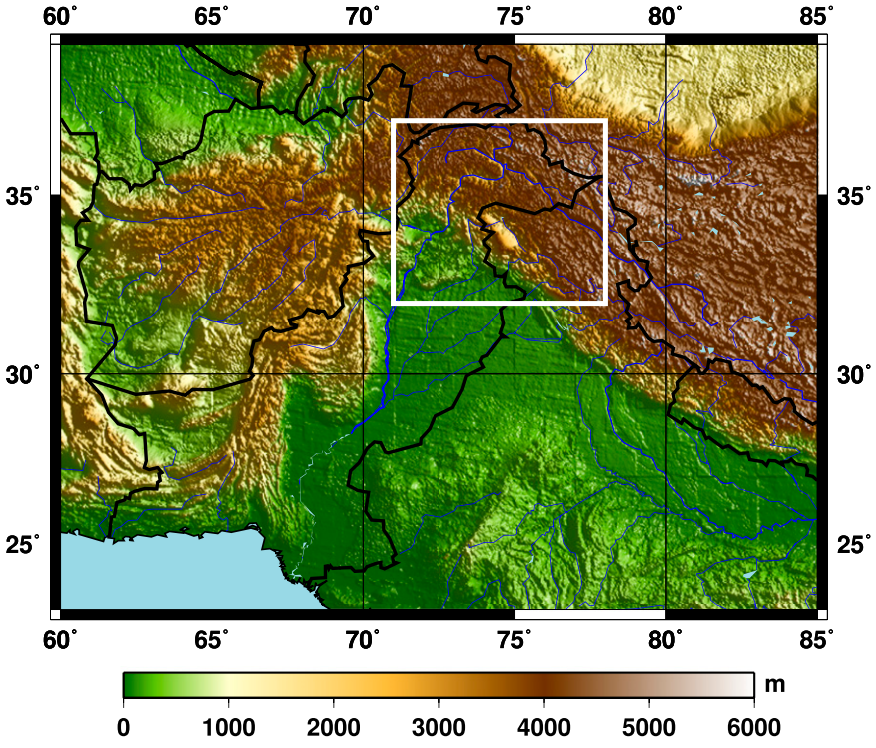

FIG. 1. Map of the Hindu Kush–Karakoram region and its surroundings. The white rectangle highlights the HKK domain.

(Immerzeel et al. 2012; Rasmussen et al. 2012). Therefore, gridded precipitation data are always biased. Although previous work has already demonstrated a link between the NAO and precipitation, here we opt for a multi-dataset approach to estimate the differences that could arise in the representation of this signal by using different large-scale data archives. We focus on the processes that are responsible for the link between the NAO and precipitation in the HKK. Particular emphasis is given to the study of the NAO-associated changes in evaporation from the main moisture reservoirs, which were not considered in previous work and can help provide a more complete view of the whole mechanism. Moreover, we address the secular variations that occurred in the NAO–precipitation signal and investigate whether the spatial shifts in the NAO variability help us to understand the observed changes, using Twentieth Century Reanalysis (20CR) data (Compo et al. 2011) to reconstruct the atmospheric variability from 1871 to the present.

This paper is structured as follows. In section 2 we discuss the datasets and the methods employed in this study. Our results are presented and discussed in sections 3 through 5, where we analyze the NAO–precipitation signal from different large-scale datasets, the importance of evaporation in the mechanism responsible for this signal, and the role of the position of the NAO COAs in determining the strength of the NAO–precipitation relationship. Final considerations and perspectives are discussed in section 6.

2. Data and methodology

a. Datasets

The precipitation datasets employed here include three rain gauge-based archives (APHRODITE, CRU, and GPCC) and the ERA-40 reanalysis. Evaporation, specific humidity, sea surface temperature (SST), and wind data from ERA-40 are also analyzed. To study multidecadal variations that occurred in the atmospheric response to the NAO, we analyze also sea level pressure (SLP) and wind fields from the 20CR, which provides information from the end of the nineteenth century.

APHRODITE produces daily precipitation data primarily obtained from a rain gauge observation network (Yatagai et al. 2012). We use the APHRO_MA (APHRODITE Monsoon Asia) V1101 dataset, characterized by a spatial resolution of 0.25° latitude/longitude, covering an area 15°S–55°N, 60°–150°E during the period 1951–2007. The GPCC dataset consists of monthly precipitation fields over land obtained from a rain gauge-based dataset. We use the GPCC version 6 release

(Schneider et al. 2011), having a spatial resolution of 0.5° latitude/longitude and a temporal coverage from 1901 to 2010. The CRU dataset consists of monthly gridded fields over land from in situ rain gauge data (Harris et al. 2013). Here we use the CRU time series version 3.21 (TS 3.21) dataset, characterized by a temporal coverage from 1901 to 2012 and a spatial resolution of 0.5° latitude/longitude. The ERA-40 reanalysis is a global atmospheric reanalysis for the period 1958–2002 developed by the ECMWF (Uppala et al. 2005). From ERA-40, we analyze total precipitation, evaporation, and SST at monthly resolution and U and V wind components, specific humidity, and 10-m wind speeds at 6-h temporal resolution. All variables are on a 1.125° latitude/longitude regular grid. Precipitation and evaporation are not assimilated in the reanalysis but are produced by the forecast model and, as such, they may be susceptible to systematic model errors (Bengtsson et al. 2004). We consider the three-dimensional specific humidity and wind fields at 1000-, 925-, 850-, 775-, 700-, 600-, 500-, 400-, 300-, and 250-hPa pressure levels. The 20CR is a global atmospheric circulation reanalysis assimilating only surface pressure data and using observed monthly SST and sea ice distributions as boundary conditions (Compo et al. 2011). We use the second version of the 20CR, available from 1871 to the present with a 2° × 2° spatial resolution, considering monthly SLP and horizontal wind fields. The 20CR data are provided by the National Oceanic and Atmospheric Administration (NOAA) Office of Oceanic and Atmospheric Research (OAR) Earth System Research Laboratory Physical Sciences Division (ESRL PSD), Boulder, Colorado (available from their website at http://www.esrl.noaa.gov/psd/).

b. Analysis methods

The whole analysis is based on seasonal (winter) average values. The winter season is defined as the period from December to March (DJFM), consistent with other studies analyzing the relationships between teleconnection patterns and precipitation in this area (Syed et al. 2006, 2010; Yadav et al. 2009b). The results presented in sections 3 and 4 refer to the period 1958–2002, during which all datasets overlap. To investigate the mechanisms by which the NAO regulates precipitation (section 4) we use the ERA-40 reanalysis. In section 5, in order to enlarge the temporal coverage to study multidecadal variations occurring in the NAO–precipitation relationship, we use the 20CR reanalysis, covering the period from winter 1872 to winter 2012.

We adopt the DJFM station-based NAO index (NAOI) [Hurrell (1995), available from the National Center for Atmospheric Research (NCAR) at http://goo.gl/opvFM]. This NAO index calculation is based on the difference between the normalized average winter SLP in Lisbon, Portugal, and in Stykkisholmur/Reykjavik, Iceland; normalization is obtained by dividing each seasonal mean pressure by the long-term (1864–1983) standard deviation, to prevent the series from being dominated by the larger variability of the northern station. We consider a winter season to be in a positive (negative) NAO phase if the NAOI is more than one standard deviation above (below) the averaged NAOI for the period 1958–2002. We have verified that our results are independent of the choice of the NAOI, by repeating the analysis using a NAO index based on empirical orthogonal functions (EOFs). We used both an index computed by NCAR (the PC-based Hurrell NAO index) and an index that we computed from ERA-40 SLP fields. The details are not reported here for the sake of conciseness.

Statistical analyses are performed mostly through 1) the computation of the correlations between the NAOI time series and other key variables, such as precipitation, evaporation, SST, wind, and moisture transport and 2) the inspection of positive and negative NAO composites of the different variables (i.e., climatological averages conditioned on the NAO phase). Correlations are computed using the Pearson linear correlation coefficient and their significance is assessed using a standard two-tailed t test. A time-shuffling method is used to assess the significance of the differences between the positive and the negative NAO composites (Pollard et al. 1987; Ciccarelli et al. 2008).

The vertically integrated water vapor (moisture) transport is computed following the approach by Chen (1985). The seasonal mean moisture transport $\overline{\mathbf{Q}}$ is given by the vertical integral (over pressure levels)

$$\overline{\mathbf{Q}} = \frac{1}{g}\int \overline{q\mathbf{v}}\, dp, \tag{1}$$

where g is the gravity acceleration, q the specific humidity, and $\mathbf{v}$ the horizontal wind; the overbar represents time average over the season. ERA-40 6-h three-dimensional fields of specific humidity and horizontal wind are used for this computation, considering only tropospheric levels (250–1000 hPa). Different variants for the choice of the upper level (here 250 hPa) exist in the literature. We have tested different choices of the upper bound and found that they do not influence our results, as the moisture content is extremely low above 250 hPa. Note, also, that in high-elevation areas the lower levels are below the earth's surface. ERA-40 fields take values very close to zero below the surface (although not exactly zero). We tested the contribution of such spurious levels in the vertical integral (1) and found that it is negligible for our purposes.

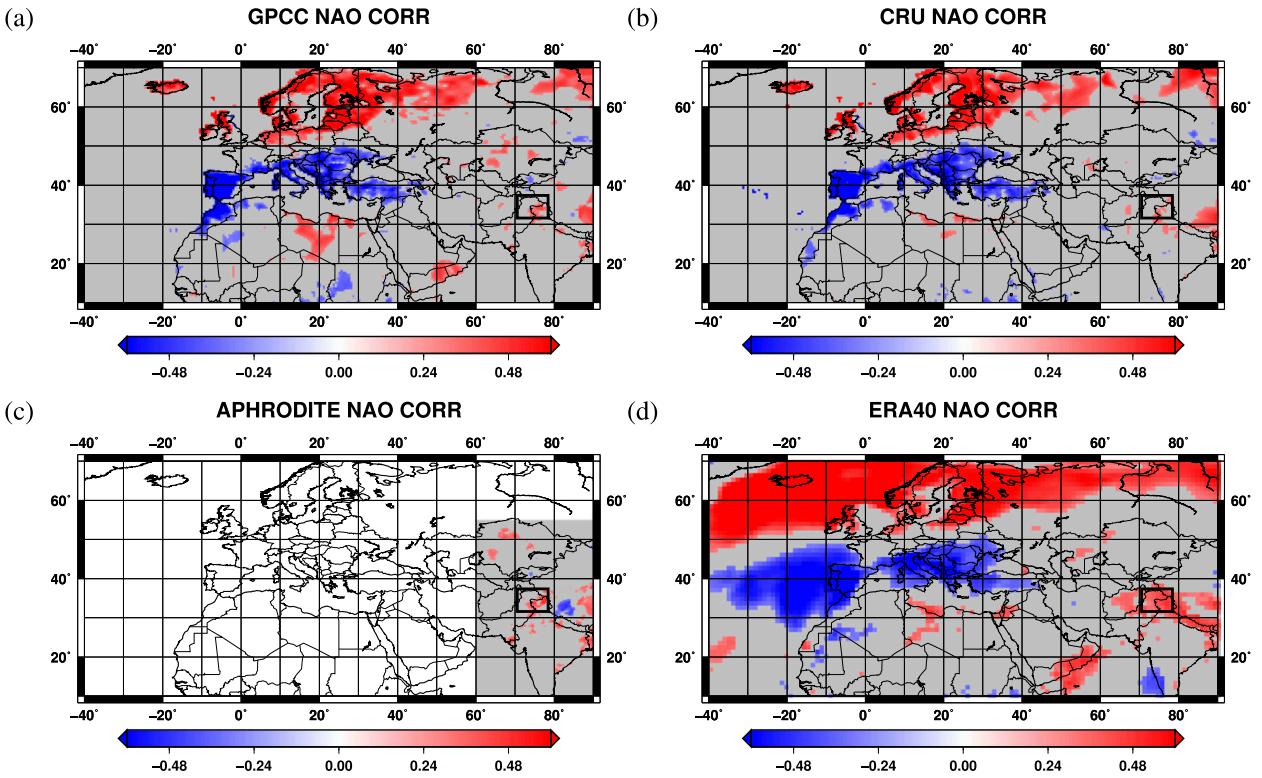

FIG. 2. Correlation coefficients between the NAOI and winter precipitation from (a) GPCC, (b) CRU, (c) APHRODITE, and (d) ERA-40 during the period 1958–2002. Colors indicate statistically significant correlations at the 95% confidence level; nonsignificant correlations are marked in gray. The black rectangle highlights the HKK region.

We investigate the slow movements of the NAO centers of action (Hilmer and Jung 2000; Lu and Greatbatch 2002), using the "angle index" introduced by Wang et al. (2012). We consider 21-yr running windows such that each subsequent window is moved over by one year. The 21-yr periods are labeled by their 11th year. For each of the 21-yr-long periods, the NAO pattern is computed as the first empirical orthogonal function (EOF1) of monthly SLP anomalies over the region 20°–80°N, 90°W–40°E. The centers of action (or nodes) of the NAO are the positions of the absolute minimum and maximum of EOF1. The sign of EOF1 is fixed so that the northern node of the NAO is always negative. The AI is computed as the angle between the axis connecting the two nodes of the NAO and its mean climatological orientation, and normalized to unit standard deviation. The AI has a positive value, and we say that the NAO has a positive tilt, when this north–south axis is tilted clockwise compared to its mean climatological orientation. In the opposite case, we say that the NAO has a negative tilt. Monthly SLP fields from the 20CR are considered for this computation. We refer to Wang et al. (2012) for the temporal evolution of the position of the NAO COAs, as well as for the spatial structure of the two nodes associated with high and low values of the AI [Figs. 1 and 3 of Wang et al. (2012) respectively].

3. NAO–precipitation signal

We explore the correlation between the NAO and precipitation by plotting the spatial distribution of the statistically significant correlations (at the 95% confidence level) between DJFM precipitation and DJFM NAOI time series (Fig. 2) and the difference between positive and negative composites of precipitation from the GPCC, CRU, APHRODITE, and ERA-40 datasets conditioned on the phase of the NAO (Fig. 3) during the period 1958–2002. The strongest signal emerging from these plots is a European precipitation dipole, discussed by Wibig (1999) and Trigo et al. (2002), in which strong positive NAO phases tend to be associated with above-average precipitation over northern Europe in winter and below-average precipitation over southern and central Europe, whereas opposite patterns of precipitation anomalies are observed during strong negative NAO phases. Another area displaying statistically significant positive correlations is located at the border between northeastern Pakistan and northwestern India, corresponding to the

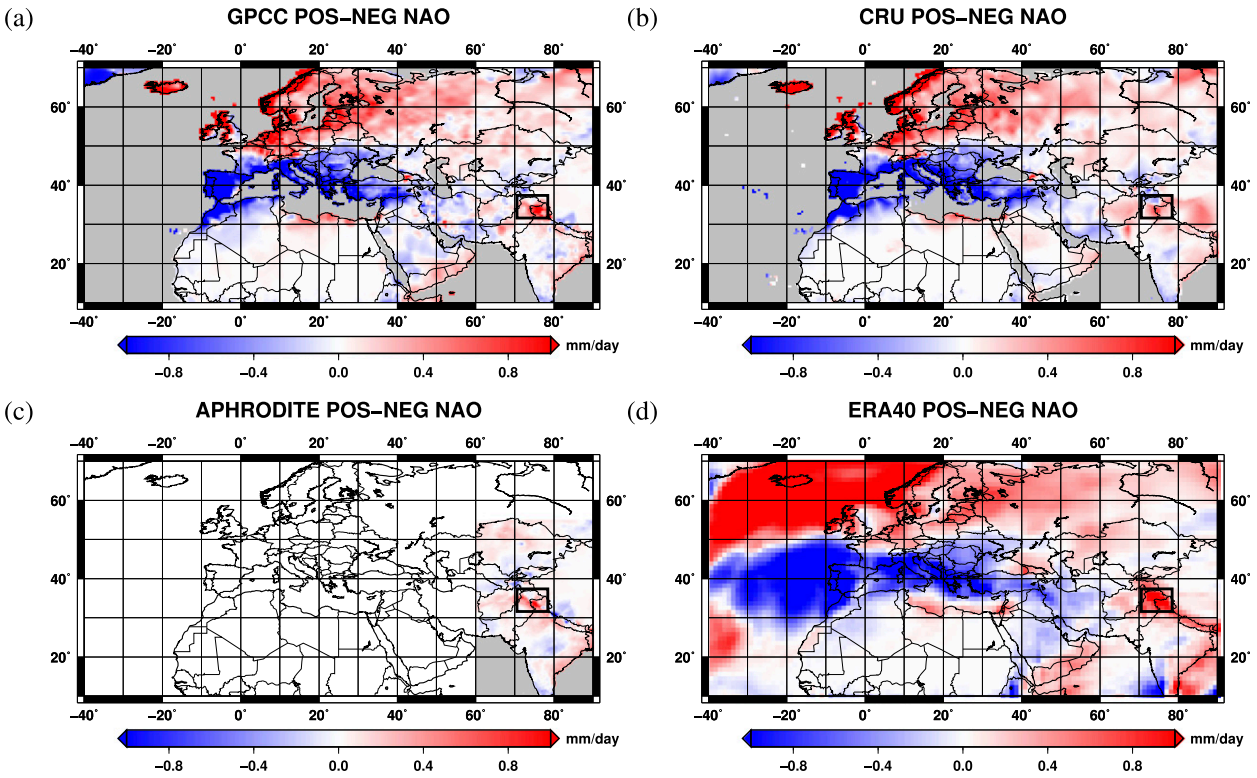

FIG. 3. Difference between the positive and the negative NAO composites of winter precipitation from (a) GPCC, (b) CRU, (c) APHRODITE, and (d) ERA-40 during the period 1958–2002. The black rectangle highlights the HKK region.

HKK region, although differences in the spatial extent arise between the datasets. In the three observation-derived datasets (GPCC, CRU, and APHRODITE) significant correlations are limited to a very small area and the weakest signal is found in CRU. Conversely, ERA-40 shows significant positive correlations over a broad area encompassing central and northern Afghanistan and Pakistan, and the greater Himalayan chain. This picture is confirmed by Fig. 3, where northern Pakistan and northern India display the strongest signal outside the European domain. All datasets show a positive (negative) precipitation anomaly during the positive (negative) NAO phase, but with differences both in the spatial extent and intensity of the anomaly. The composites in this area are statistically significant in ERA-40, while they are not in the three observation-derived datasets.

These results are consistent with previous works. Syed et al. (2010) observed that the nonsignificance of the NAO–precipitation signal in this area is due to the high variability of precipitation. These regions receive low precipitation amounts and exhibit high noise levels (Palazzi et al. 2013). The weak NAO–precipitation signal suggests that the NAO is not the only factor regulating precipitation, but there is high interannual variability owing to other sources, including other teleconnection patterns such as ENSO (Syed et al. 2006, 2010; Yadav et al. 2009b, 2010; Dimri 2013), Indian Ocean sea surface temperatures (Yadav et al. 2007), convection over the warm pool region (Yadav et al. 2009a), and random atmospheric variability. Differences between the datasets highlight current problems in having reliable precipitation estimates in this region and the importance of using multiple datasets to estimate uncertainties. The lower correlation signal in station-based datasets, compared to ERA-40, may be associated with the underestimation of total precipitation in the observations (Palazzi et al. 2013) where winter snowfall is not adequately captured. However, we note that reanalysis precipitation outputs should be treated with care, as they are susceptible to model errors and inhomogeneities in the data used in the assimilation procedure.

4. NAO-related variability of moisture transport and evaporation

The secondary maximum of the Asian subtropical jet stream located climatologically over northern Egypt and Saudi Arabia [the Middle East jet stream (MEJS)] has been recognized as an important factor in determining

climate over southern Asia, and the NAO can exert its effects on this region through modifications of the jet (Yang et al. 2004). Yadav et al. (2009b) suggested that the NAO regulates winter precipitation in northern India by strengthening the MEJS from North Africa to southeastern Asia during its positive phase. To study the effects of the NAO on tropospheric westerlies over this region, in the vertical cross section of Fig. 4 we show the correlation coefficients between the NAOI and zonal wind (averaged between 40° and 70°E) in the Northern Hemisphere. This meridional band corresponds to the longitudes of greater importance for the transport of humidity toward the HKK (see below). Significant positive correlations are found from the lower to the higher troposphere at latitudes between 20° and 30°N, where the climatological jet is located. The jet stream core in the upper troposphere (around 200 hPa) is intensified and slightly shifted to the north during the positive NAO phase. The strengthening of the westerlies at these latitudes is marked throughout the troposphere and weakens slightly only at lower levels (below 800–850 hPa), where surface effects become important and the mean circulation increasingly deviates from the zonal flow. NAO-related changes of middle tropospheric westerlies are consistent with the deeper 500-hPa trough observed by Syed et al. (2006, 2010), highlighting the link between their findings and the ones by Yadav et al. (2009b).

We explore to what extent this anomaly in westerly winds affects moisture transport toward the HKK. A first step is to identify the major sources of the humidity transported to the HKK region. Figure 5a shows the climatology of vertically integrated moisture transport (vectors) superimposed on the spatial map of the significant correlations between the NAOI and the intensity of moisture transport (i.e., the modulus of the transport vector). The climatology shows that moisture, originating mainly from the northern Arabian Sea and the Red Sea, is transported toward the HKK through the Persian Gulf. This result is consistent with Yadav et al. (2010). A comparatively smaller moisture contribution comes from the Mediterranean area, although, on average, moisture from that area deviates northeastwardly and affects mainly the regions north of the HKK. As expected, in the correlation map (colored filled contours in Fig. 5a) significant positive correlations occur over central-western Europe, while negative correlations occur across all of the Mediterranean area, as shown by Hurrell (1995). This map also shows that the intensity of moisture transport from the Arabian Peninsula toward Pakistan and western India is significantly larger during the positive NAO phase. The strengthening of moisture transport in this region during the positive NAO phase may sustain wetter than normal conditions in winter in

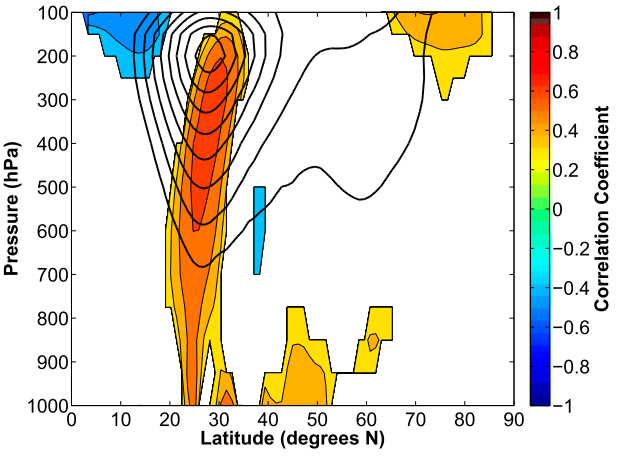

FIG. 4. Correlation coefficients (filled colored contours) between the NAOI and winter zonal wind averaged over longitudes between 40° and 70°E during the period 1958–2002. Only correlations statistically significant at the 95% confidence level are reported. Climatology (1958–2002) of winter zonal wind (black contours) averaged over longitudes between 40° and 70°E, identifying the position of the Middle East jet stream: only values above 10 m s^{-1} are reported. Contour interval is 5 m s^{-1}.

the HKK, as discussed by Syed et al. (2010). Significant positive correlations are found also over a thin zonal strip in eastern Africa between about 15° and 25°N. The contiguity of this region to the Arabian Peninsula may suggest an interdependence between the two signals, but, as shown by the vectors of moisture transport superimposed on the correlation map, on average humidity from this region deviates southward and does not flow directly into the Arabian Peninsula.

While changes in tropospheric circulation play a major role in determining the enhanced moisture transport from Arabia to Pakistan during positive NAO periods, wind is not the only variable influencing moisture transport. In Fig. 5b we show the difference between positive and negative NAO composites of evaporation: during the positive NAO phase, enhanced evaporation occurs from the Red Sea, the Persian Gulf, the northern Arabian Sea, and the southeastern Mediterranean Sea. As mentioned above, these basins constitute the major moisture sources for the HKK. The evaporation anomaly found in the southeastern Mediterranean Sea is associated with dry air conditions during the positive NAO phase, as discussed by Hurrell (1995). The evaporation signal from the Red Sea, the Persian Gulf, and the northern Arabian Sea is associated with coherent signals in surface wind speed and SST, as shown in Figs. 5c and 5d, respectively. During the positive NAO phase, ERA-40 shows high surface wind speed over the Red Sea (note the good correspondence with evaporation anomalies), the Persian Gulf (significant correlations in the southern

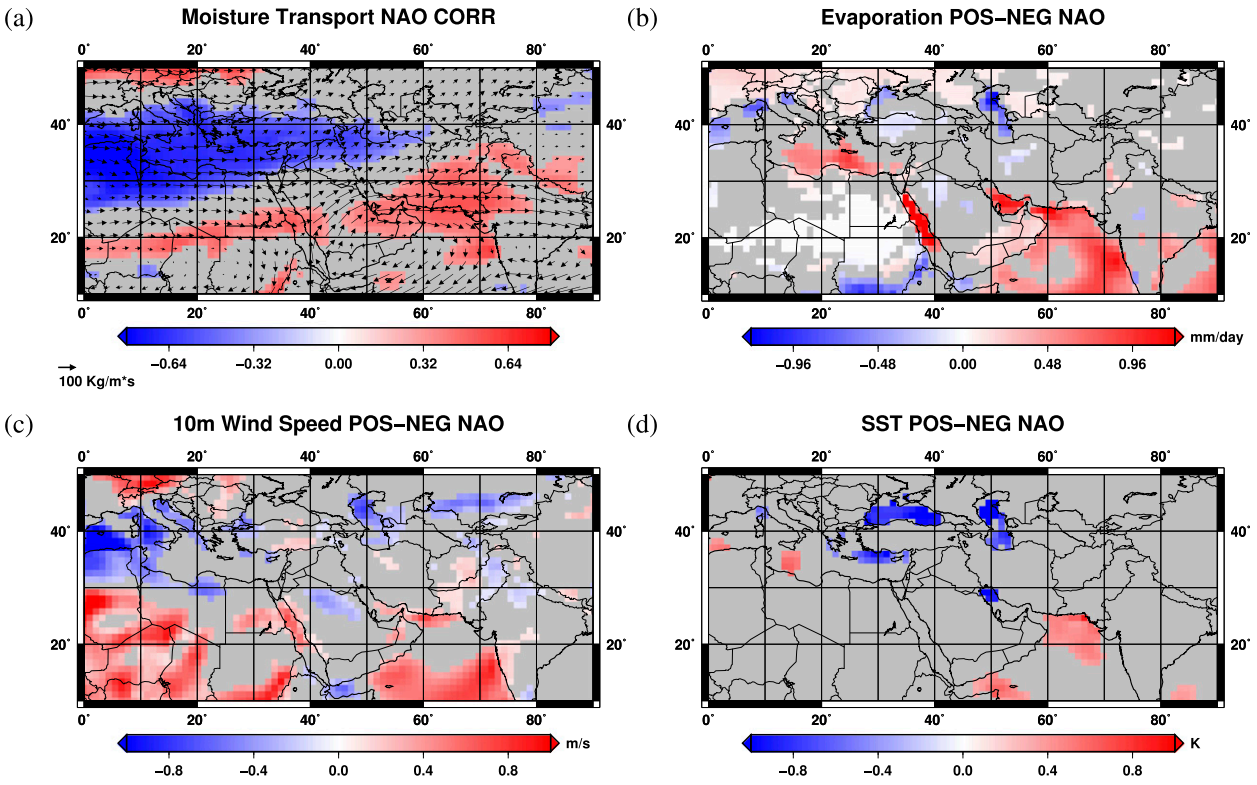

FIG. 5. (a) Climatology of moisture transport during winter (vectors) and correlation coefficients between the NAOI and the intensity of moisture transport (color map). Colors are used for statistically significant correlations at the 95% confidence level; gray indicates nonsignificant correlations. (b)–(d) Difference between the positive and the negative NAO composites of evaporation, 10-m wind speed, and SST, respectively. Colors indicate statistically significant values at the 95% confidence level; gray indicates nonsignificant values. All panels refer to the period 1958–2002.

part where the evaporation anomaly is stronger than elsewhere), and the northern Arabian Sea (significant correlations in the northernmost part of the region and south of about 20°–15°N). High SSTs occur in a portion of the northern Arabian Sea. The whole picture provided by Figs. 5c and 5d matches well with the evaporation signal reported in Fig. 5b. We note that the SST anomaly in the northern Arabian Sea is relatively confined, and we did not find a clear explanation for this effect either in the literature or in the results of our analysis. The results reported here suggest that the dominant path through which the NAO induces higher evaporation is the intensification of surface winds. This intensification might ensue from the NAO-induced strengthening of tropospheric westerlies over this region, as discussed above (see Fig. 4), although the link between the two is not trivial given the strong influence of surface conditions.

5. Nonstationarity of the NAO–precipitation teleconnection

Yadav et al. (2009b) observed for the first time, using station data from the Indian Meteorological Department (IMD), that the relationship between the NAO and precipitation in northwest India underwent multidecadal changes during the twentieth century. To see if these changes are detectable also in the large-scale datasets used here, in Fig. 6 we show the sliding correlations over 21-yr moving windows between the NAOI and the time series of precipitation averaged in the HKK domain from GPCC, CRU, APHRODITE, and ERA-40. The HKK domain is defined, as in Palazzi et al. (2013), in the range 32°–37°N, 71°–78°E and is highlighted by the white rectangle in Fig. 1. Note that this domain slightly differs from the one used in Yadav et al. (2009b), who focused on a larger portion of northwestern India and did not include northern Pakistan. The various datasets have different temporal coverages, but they all show consistent changes in the NAO–precipitation relationship during their overlapping periods. Correlation coefficients between the NAO and precipitation are significant in the period between 1940 and 1980, whereas they are not significant after 1980 and between 1920 and 1940. The two datasets extending to the first years of the twentieth century show a stronger signal before 1920 with respect to the following decade (the correlations are statistically significant

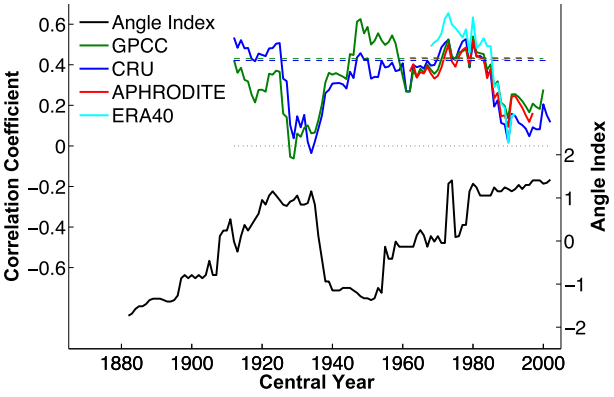

FIG. 6. Sliding correlations on 21-yr moving windows between the NAOI and the time series of precipitation averaged in the HKK domain (71°–78°N, 32°–37°E) from GPCC (green), CRU (blue), APHRODITE (red), and ERA-40 (cyan). Dashed lines indicate the 95% significance level and the dotted line indicates zero correlation. The black line is the time series of the AI. Sliding correlations and the AI have different *y* axes on the left and right side respectively. Values are plotted at the 11th year of each 21-yr window.

in CRU but not in GPCC) and seem to suggest a decline of the NAO control on precipitation during these years. However, it is worth pointing out that precipitation estimates are less and less reliable as we move back to the beginning of the century, as the number of stations in this area decreases and the gridded datasets are obtained by interpolating data from stations quite far from each other. As a further check, we have computed the spatial distribution of the correlations between the NAOI and precipitation from the different datasets during the periods 1958–79 and 1981–2002, that is, before and after 1980 (not shown here). In the HKK region, all datasets indicate a more widespread area of statistically significant correlations during 1958–79 than during 1981–2002 (when significant correlations almost disappear), consistent with the drop of the correlation occurring around 1980 shown in Fig. 6. These changes in the intensity of the NAO–precipitation correlations are in good agreement with the results of Yadav et al. (2009b), giving robustness to our findings and showing that the large-scale datasets describe multidecadal variations in a consistent manner.

Figure 6 shows the time series of the angle index, which measures the spatial displacements of the NAO pattern in the North Atlantic on decadal time scales. The temporal evolution of the AI shows interesting similarities with the time series of the correlation between the NAO and precipitation, and the two seem to evolve in antiphase: in the two periods with nonsignificant correlations (1920–40 and 1980 onward) the AI shows the highest values (i.e., the NAO has a positive tilt). Conversely, the period with significant correlations (1940–80) is characterized by lower values of the AI, which was strongly negative before the mid-1950s (when GPCC shows its highest correlations) and approximately zero afterward. At the beginning of the twentieth century, when CRU and GPCC suggest a weakening of the NAO–precipitation relationship, the AI is moving from negative to positive values. As discussed in section 3, there are sources of variability other than the NAO for precipitation in this area. These factors add noise to the record of sliding correlations, potentially worsening the synchronization with the time series of the AI. However, our results support the view that the position of the NAO COAs regulates the strength of the NAO–precipitation relationship in the HKK region. In particular, Fig. 6 suggests that, when the NAO has a positive tilt, the NAO–precipitation correlation is weaker, whereas suitable conditions for the NAO–precipitation correlation are found when the NAO shows a negative—or at least very small—tilt.

Previous work showed that shifts of the NAO COAs have significant implications for the circulation response to the NAO phase in the North Atlantic and European sectors (Jung et al. 2003; Wang et al. 2012), with possible implications also outside these domains. In section 4 we discussed how the NAO control on precipitation in the HKK occurs through the regulation of westerlies in the region of the MEJS, including changes in evaporation. To investigate whether the different configurations of the spatial pattern of the NAO have an effect on the way the NAO regulates westerlies in this region, we compute composites of the correlation coefficients between the NAOI and 250-hPa zonal winds conditioned on periods when the AI is high or low (i.e., more than one standard deviation above or below the mean). To have a larger temporal coverage, from winter 1872 to winter 2012, we use the 20CR wind data. Correlation fields are computed on 21-yr windows, to be consistent with the definition of the AI. Results are shown in Figs. 7a and 7c for low and high values of the AI respectively. The dots highlight grid points where the correlation coefficients are statistically significant at the 95% confidence level in all 21-yr periods considered in the composite. The figures show four domains of influence of the NAO: negative values are found over Greenland and over a zonal band extending from the southern United States to Mediterranean Europe, while positive values are found at about 60°N from western Canada to Scandinavia and to the south from tropical North Atlantic to southeastern Asia. The latter region corresponds to the intensification of the MEJS. When the NAO has a negative tilt (Fig. 7a), significant correlations over Greenland are displaced more to the west and the bands of positive and

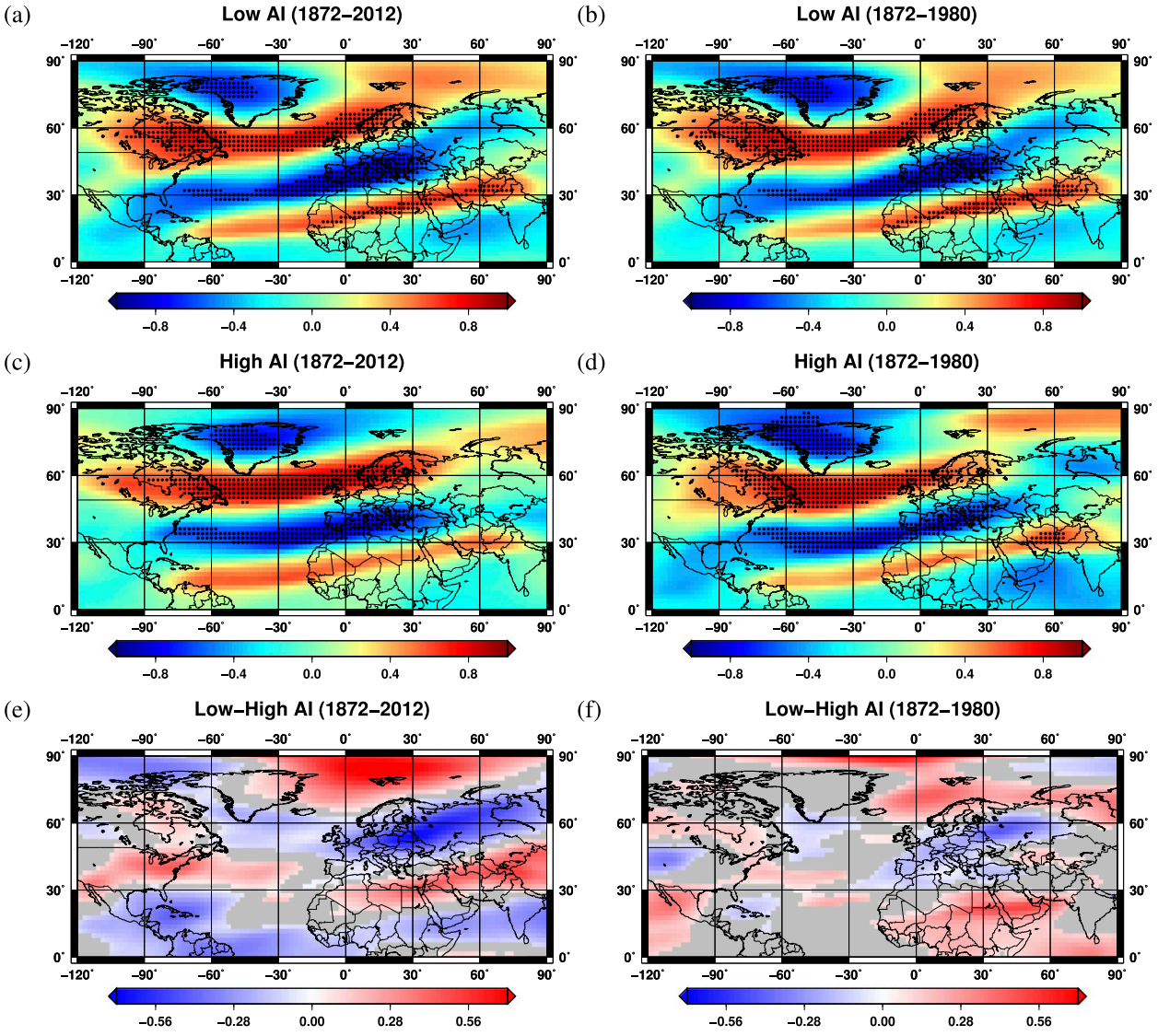

FIG. 7. Composites of the correlation fields between the NAOI and 250-hPa zonal wind corresponding to (a) low and (c) high values of the AI for the period 1872–2012. Correlation fields are computed on 21-yr windows to be consistent with the definition of the AI. Dots indicate grid points where the correlation coefficients are statistically significant at the 95% confidence level in all the 21-yr periods considered in the composite. (e) Difference between the composites at low and high AI, (a) minus (c). Colors indicate statistically significant values at the 95% confidence level; gray indicates nonsignificant values. The significance of the difference is assessed using a time-shuffling method. (b),(d),(f) As in (a),(c), and (e), but for the period 1872–1980.

negative correlation in the extratropical North Atlantic have a more southwest–northeast orientation. In the region of the MEJS, significant positive correlations are found from North Africa to Pakistan, indicating that the NAO exerts a strong control on the jet mainly when the AI is low. When the NAO has a positive tilt (Fig. 7c), negative correlations over Greenland are displaced more to the east, and the two bands of significant correlations in the extratropical North Atlantic have a more zonal orientation. During these periods, characterized by high values of the AI, the NAO exerts only a weak control on the MEJS, with a drop of the statistical significance of the signal. In Fig. 7e we show the difference between Figs. 7a and 7c to further highlight the changes occurring between periods of low and high values of the AI. The significance of the difference is assessed using a time-shuffling method (Ciccarelli et al. 2008). The significant positive values occurring in the region of the MEJS indicate that differences between Figs. 7a and 7c in this area are large enough not to be just due to random sampling differences. The fact that, when the AI is high, the NAO does not project—or projects weakly—onto

the MEJS can explain why the NAO–precipitation relationship weakens. Conversely, suitable conditions for a significant NAO–precipitation signal occur when the AI is low because the NAO exerts a strong control on the jet.

Figures 7a, 7c, and 7e show the results obtained by considering all winters covered by 20CR data (1872–2012). After 1980, the atmospheric response to ENSO has strengthened; ENSO has started to influence also the intensity and position of the MEJS and consequently precipitation in the HKK. A stronger control of ENSO could weaken the NAO signature. Since this period shows high values of the AI, one might ask if the weaker signal in Fig. 7c could ensue from this change in ENSO. To investigate this issue, Figs. 7b, 7d, and 7f were obtained exactly in the same way as Figs. 7a, 7c, and 7e, but excluding the years after 1980 from the analysis. We anticipate weaker differences between low and high AI values during the period 1872–1980 than during 1872–2012 since we are excluding periods of strong positive AI. However, also in this case the differences in the NAO control of the jet associated with opposite values of the AI are evident. In Fig. 7d (high AI), significant positive correlations are found in a limited area over Iran, but the overall signal in the region of the MEJS is weak and nonsignificant. In Fig. 7b (low AI), the signal is stronger and statistically significant from North Africa to Pakistan. The differences between low and high AI shown in Fig. 7f are not significant over Iran, but they are significant over North Africa and Saudi Arabia. From these results, we can state that the differences in the relationship between the NAO and the MEJS observed when the AI is high or low are independent of the changes that could have occurred in the period post-1980, and thus they are not a direct product of ENSO.

The AI is a measure of the relative position of the NAO COAs and considers both northern and the southern node of the NAO. To understand if one of the two nodes is more important than the other, we have repeated the same analysis presented in Fig. 7 but using indices measuring the position of a single NAO COA instead of the AI. The results (not shown here) are consistent with the considerations drawn from Fig. 7 for the AI and indicate that both indices play a role in determining the strength of the NAO influence on the jet.

6. Discussion and conclusions

Winter precipitation in the Hindu Kush–Karakoram (HKK), an essential water input for the area, is associated with the arrival of westerly perturbations, the western weather patterns (WWPs), originating from the Mediterranean and northeastern Atlantic regions. The existence of correlations between the NAO and winter precipitation in the HKK is well known (Syed et al. 2006, 2010; Yadav et al. 2009b). Here we have used an ensemble of large-scale precipitation datasets, showing that they coherently reproduce the NAO–precipitation link, and we have discussed the importance of evaporation anomalies in the processes responsible for the relationship between the NAO and winter precipitation in the HKK. We have also addressed the issue related to the multidecadal variations occurring in the NAO–precipitation relationship and have argued that these changes are related to the spatial structure of the NAO pattern in the North Atlantic basin.

Consistent with previous studies, our analysis of the relationship between the NAO index and precipitation estimates from three gridded observation-based datasets (APHRODITE, CRU, and GPCC) and from the ERA-40 reanalysis confirms that the NAO influences the amount of precipitation in the HKK. All datasets considered here show that years in the positive (negative) NAO phase are characterized by above (below) normal precipitation over the target area in winter (December–March). Differences among the datasets arise in the spatial extent, intensity, and significance level of the NAO-associated precipitation anomalies. Compared to the three observation-based datasets, ERA-40 shows a stronger link between the NAO and precipitation, which is statistically significant over a broader area extending from northern Afghanistan to northern India.

The relationship between precipitation and the NAO is maintained through the control exerted by the NAO on the westerlies in the region of the Middle East jet stream (MEJS), from North Africa to southeastern Asia. At longitudes between 40° and 70°E, where the majority of moisture transport toward the HKK takes place, the intensification of the westerlies during the positive NAO phase is evident from the upper-tropospheric jet to the lower-level westerlies. The stronger jet intensifies the WWPs (Yadav et al. 2009b) and faster westerlies in the middle to lower troposphere intensify moisture transport toward the HKK (Syed et al. 2010). In addition to this, we have shown that evaporation plays an important role in this mechanism. Our analysis suggests that the main moisture sources for precipitation in the HKK are in the northern Arabian Sea, the Red Sea, the Persian Gulf, and, to a lesser extent, the Mediterranean Sea. During the positive NAO phase, enhanced evaporation occurs from these reservoirs. Evaporation anomalies from the first three basins are mainly related to higher surface wind speed. We suggest that surface wind anomalies might be associated with the strengthening of westerlies in this region during the positive NAO phase, even if the link with upper-level circulation is not trivial owing to the strong effects of surface

topography. The increased humidity arising from evaporation combines with the intensification of westerlies to give enhanced moisture transport toward the HKK. As a consequence, wetter conditions are found over northern Pakistan and northern India and larger precipitation amounts are released as the western weather patterns reach this region.

The precipitation datasets used in this study show significant multidecadal variations in the relationship between the NAO and precipitation, consistent with observations of Yadav et al. (2009b). We have used the NAO angle index (AI) introduced by Wang et al. (2012) to measure the slow movements of the NAO centers of action. Our results show that high values of the AI (positive tilt of the NAO) are associated with nonsignificant correlations between the NAO and precipitation in the HKK, while significant correlations occur when the AI is negative. Shifts in the position of the NAO COAs have significant implications for the NAO-associated circulation anomalies in the troposphere. In particular, when the AI is low, the NAO exerts a strong control on the MEJS and, as a consequence, the mechanism of regulation of the HKK precipitation by the NAO is activated. The opposite occurs when the AI is high. The AI considered here is one of the possible indices measuring the changes in the NAO spatial pattern, and others can be defined that capture slightly different features (such as considering only one of the two centers of action). What is important here is that changes in the spatial structure of the NAO pattern can be crucial in determining the strength of the relationship between the NAO and other climatic parameters, and as a consequence in determining precipitation in the HKK.

Acknowledgments. The authors thank Paolo Davini for prolonged and constructive discussions, which helped to significantly improve this work, and the anonymous reviewers of a previous version of the manuscript for their useful and constructive comments. This work was funded by the NextData project of the Italian Ministry of Education, University and Research. We acknowledge the institutions and the teams responsible for the creation and publication of the GPCC, APHRODITE, CRU, TRMM, ERA-40, and 20CR archives. ERA-40 data have been obtained from the ECMWF Data Server. Support for the 20CR Project dataset is provided by the U.S. Department of Energy, Office of Science Innovative and Novel Computational Impact on Theory and Experiment (DOE INCITE) program, and Office of Biological and Environmental Research (BER), and by the National Oceanic and Atmospheric Administration Climate Program Office.

REFERENCES

Ambaum, M. H., B. J. Hoskins, and D. B. Stephenson, 2001: Arctic Oscillation or North Atlantic Oscillation? *J. Climate,* **14,** 3495–3507, doi:10.1175/1520-0442(2001)014<3495:AOONAO>2.0.CO;2.

Archer, D. R., and H. J. Fowler, 2004: Spatial and temporal variations in precipitation in the Upper Indus Basin, global teleconnections and hydrological implications. *Hydrol. Earth Syst. Sci.,* **8,** 47–61, doi:10.5194/hess-8-47-2004.

Bengtsson, L., K. I. Hodges, and S. Hagemann, 2004: Sensitivity of large-scale atmospheric analyses to humidity observations and its impact on the global water cycle and tropical and extratropical weather systems in ERA-40. *Tellus,* **56A,** 202–217, doi:10.1111/j.1600-0870.2004.00053.x.

Bookhagen, B., and D. W. Burbank, 2010: Toward a complete Himalayan hydrological budget: Spatiotemporal distribution of snowmelt and rainfall and their impact on river discharge. *J. Geophys. Res.,* **115,** F03019, doi:10.1029/2009JF001426.

Chen, T.-C., 1985: Global water vapor flux and maintenance during FGGE. *Mon. Wea. Rev.,* **113,** 1801–1819, doi:10.1175/1520-0493(1985)113<1801:GWVFAM>2.0.CO;2.

Ciccarelli, N., J. von Hardenberg, A. Provenzale, C. Ronchi, A. Vargiu, and R. Pelosini, 2008: Climate variability in northwestern Italy during the second half of the 20th century. *Global Planet. Change,* **63,** 185–195, doi:10.1016/j.gloplacha.2008.03.006.

Compo, G. P., and Coauthors, 2011: The Twentieth Century Reanalysis Project. *Quart. J. Roy. Meteor. Soc.,* **137,** 1–28, doi:10.1002/qj.776.

Deser, C., 2000: On the teleconnectivity of the ''Arctic Oscillation.'' *Geophys. Res. Lett.,* **27,** 779–782, doi:10.1029/1999GL010945.

Dimri, A., 2013: Relationship between ENSO phases with northwest India winter precipitation. *Int. J. Climatol.,* **33,** 1917–1923, doi:10.1002/joc.3559.

Feldstein, S. B., 2002: The recent trend and variance increase of the annular mode. *J. Climate,* **15,** 88–94, doi:10.1175/1520-0442(2002)015<0088:TRTAVI>2.0.CO;2.

Gillett, N. P., H. F. Graf, and T. J. Osborn, 2003: Climate change and the North Atlantic Oscillation. *The North Atlantic Oscillation: Climatic Significance and Environmental Impact, Geophys. Monogr.,* Vol. 134, Amer. Geophys. Union, 193–209.

Harris, I., P. Jones, T. Osborn, and D. Lister, 2013: Updated high-resolution grids of monthly climatic observations—The CRU TS3.10 dataset. *Int. J. Climatol.,* **34,** 623–642, doi:10.1002/joc.3711.

Hilmer, M., and T. Jung, 2000: Evidence for a recent change in the link between the North Atlantic Oscillation and Arctic sea ice export. *Geophys. Res. Lett.,* **27,** 989–992, doi:10.1029/1999GL010944.

Hurrell, J. W., 1995: Decadal trends in the North Atlantic Oscillation: Regional temperatures and precipitation. *Science,* **269,** 676–679, doi:10.1126/science.269.5224.676.

——, Y. Kushnir, G. Ottersen, and M. Visbeck, 2003: An overview of the North Atlantic Oscillation. *The North Atlantic Oscillation: Climatic Significance and Environmental Impact, Geophys. Monogr.,* Vol. 134, Amer. Geophys. Union, 1–35.

Immerzeel, W. W., F. Pellicciotti, and A. B. Shrestha, 2012: Glaciers as a proxy to quantify the spatial distribution of precipitation in the Hunza basin. *Mt. Res. Dev.,* **32,** 30–38, doi:10.1659/MRD-JOURNAL-D-11-00097.1.

Jung, T., M. Hilmer, E. Ruprecht, S. Kleppek, S. K. Gulev, and O. Zolina, 2003: Characteristics of the recent eastward shift of

interannual NAO variability. *J. Climate,* **16,** 3371–3382, doi:10.1175/1520-0442(2003)016<3371:COTRES>2.0.CO;2.

Lu, J., and R. J. Greatbatch, 2002: The changing relationship between the NAO and Northern Hemisphere climate variability. *Geophys. Res. Lett.,* **29,** 1148, doi:10.1029/2001GL014052.

Luo, D., Z. Zhu, R. Ren, L. Zhong, and C. Wang, 2010: Spatial pattern and zonal shift of the North Atlantic Oscillation. Part I: A dynamical interpretation. *J. Atmos. Sci.,* **67,** 2805–2826, doi:10.1175/2010JAS3345.1.

Pal, I., A. W. Robertson, U. Lall, and M. A. Cane, 2014: Modeling winter rainfall in northwest India using a hidden Markov model: Understanding occurrence of different states and their dynamical connections. *Climate Dyn.,* doi:10.1007/s00382-014-2178-5, in press.

Palazzi, E., J. von Hardenberg, and A. Provenzale, 2013: Precipitation in the Hindu-Kush Karakoram Himalaya: Observations and future scenarios. *J. Geophys. Res.,* **118,** 85–100, doi:10.1029/2012JD018697.

Pinto, J. G., and C. C. Raible, 2012: Past and recent changes in the North Atlantic Oscillation. *Wiley Interdiscip. Rev.: Climate Change,* **3,** 79–90, doi:10.1002/wcc.150.

Pollard, E., K. Lakhani, and P. Rothery, 1987: The detection of density-dependence from a series of annual censuses. *Ecology,* **68,** 2046–2055, doi:10.2307/1939895.

Rasmussen, R., and Coauthors, 2012: How well are we measuring snow: The NOAA/FAA/NCAR winter precipitation test bed. *Bull. Amer. Meteor. Soc.,* **93,** 811–829, doi:10.1175/BAMS-D-11-00052.1.

Schneider, U., A. Becker, P. Finger, A. Meyer-Christoffer, B. Rudolf, and M. Ziese, 2011: GPCC full data reanalysis version 6.0 at 0.5: Monthly land-surface precipitation from rain-gauges built on GTS-based and historic data. Global Precipitation Climatology Centre at Deutscher Wetterdienst, doi:10.5676/DWD_GPCC/FD_M_V6_050.

Syed, F. S., F. Giorgi, J. S. Pal, and M. P. King, 2006: Effect of remote forcings on the winter precipitation of central southwest Asia. Part 1: Observations. *Theor. Appl. Climatol.,* **86,** 147–160, doi:10.1007/s00704-005-0217-1.

——, ——, ——, and K. Keay, 2010: Regional climate model simulation of winter climate over central-southwest Asia, with emphasis on NAO and ENSO effects. *Int. J. Climatol.,* **30,** 220–235, doi:10.1002/joc.1887.

Thompson, D. W., and J. M. Wallace, 2001: Regional climate impacts of the Northern Hemisphere annular mode. *Science,* **293,** 85–89, doi:10.1126/science.1058958.

——, ——, and G. C. Hegerl, 2000: Annular modes in the extratropical circulation. Part II: Trends. *J. Climate,* **13,** 1018–1036, doi:10.1175/1520-0442(2000)013<1018:AMITEC>2.0.CO;2.

Trigo, R. M., T. J. Osborn, and J. M. C. Real, 2002: The North Atlantic Oscillation influence on Europe: Climate impacts and associated physical mechanisms. *Climate Res.,* **20,** 9–17, doi:10.3354/cr020009.

Uppala, S. M., and Coauthors, 2005: The ERA-40 Re-Analysis. *Quart. J. Roy. Meteor. Soc.,* **131,** 2961–3012, doi:10.1256/qj.04.176.

Wallace, J. M., 2000: North Atlantic Oscillation/annular mode: Two paradigms—One phenomenon. *Quart. J. Roy. Meteor. Soc.,* **126,** 791–805, doi:10.1002/qj.49712656402.

Wang, Y.-H., G. Magnusdottir, H. Stern, X. Tian, and Y. Yu, 2012: Decadal variability of the NAO: Introducing an augmented NAO index. *Geophys. Res. Lett.,* **39,** L21702, doi:10.1029/2012gl053413.

Wibig, J., 1999: Precipitation in Europe in relation to circulation patterns at the 500-hPa level. *Int. J. Climatol.,* **19,** 253–269, doi:10.1002/(SICI)1097-0088(19990315)19:3<253::AID-JOC366>3.0.CO;2-0.

Yadav, R. K., K. Rupa Kumar, and M. Rajeevan, 2007: Role of Indian Ocean sea surface temperatures in modulating northwest Indian winter precipitation variability. *Theor. Appl. Climatol.,* **87,** 73–83, doi:10.1007/s00704-005-0221-5.

——, ——, and ——, 2009a: Out-of-phase relationships between convection over northwest India and warm pool region during the winter season. *Int. J. Climatol.,* **29,** 1330–1338, doi:10.1002/joc.1783.

——, ——, and ——, 2009b: Increasing influence of ENSO and decreasing influence of AO/NAO in the recent decades over northwest India winter precipitation. *J. Geophys. Res.,* **114,** D12112, doi:10.1029/2008JD011318.

——, J. H. Yoo, F. Kucharski, and M. A. Abid, 2010: Why is ENSO influencing northwest India winter precipitation in recent decades? *J. Climate,* **23,** 1979–1993, doi:10.1175/2009JCLI3202.1.

——, K. R. Kumar, and M. Rajeevan, 2012: Characteristic features of winter precipitation and its variability over northwest India. *J. Earth Syst. Sci.,* **121,** 611–623, doi:10.1007/s12040-012-0184-8.

Yang, S., K. Lau, S. Yoo, J. Kinter, K. Miyakoda, and C. Ho, 2004: Upstream subtropical signals preceding the Asian summer monsoon circulation. *J. Climate,* **17,** 4213–4229, doi:10.1175/JCLI3192.1.

Yatagai, A., K. Kamiguchi, O. Arakawa, A. Hamada, N. Yasutomi, and A. Kitoh, 2012: APHRODITE: Constructing a long-term daily gridded precipitation dataset for Asia based on a dense network of rain gauges. *Bull. Amer. Meteor. Soc.,* **93,** 1401–1415, doi:10.1175/BAMS-D-11-00122.1.